Thermal resistance of silicon point contacts

L. Weber, E. Gmelin, and H. J. Queisser
Max-Planck-Institut für Festkörperforschung, Postfach 80 06 65, D-7000 Stuttgart 80, Federal Republic of Germany
(Received 6 March 1989)

We investigate thermal transport on microcontacts established between two silicon wedges. The measurements are carried out with a variable contact radius of 0.3–2 μm at temperatures from 2 to 300 K. The measured thermal resistance is used to calculate the contact radius with an accuracy better than 50%. Comparison of electrical and thermal transport indicates the existence of a tunnel barrier between the contact legs. Electrical measurements are therefore unreliable to determine the contact size.

I. INTRODUCTION

Measurements on structures with small geometrical dimensions are an important tool of current solid-state research. Point-contact spectroscopy provides information about the interaction of electrons and low-energy excitations in solids. Transport measurements on point contacts give insight into microscopic transport mechanisms. Whereas the electrical resistance of metals and metallic alloys has been studied quite extensively by point-contact spectroscopy,[1] other transport properties, such as thermoelectric power[2] or heat conductivity,[3] have only scarcely been investigated. Recent measurements on silicon microcontacts showed a large decrease of the thermoelectric power when the contact area was reduced.[4] This behavior was interpreted as a reduction of the phonon-drag part of the thermoelectric power due to phonon boundary scattering. Earlier measurements on silicon point contacts proved ballistic transport of charge carriers by investigation of asymmetric Joule-heat production.[5]

In this work, we present for the first time measurements of the thermal resistance of silicon point contacts. Electrical and thermal resistance of the contact are measured simultaneously and compared with each other. Measurements are carried out with variable contact load in the extended temperature range from $T=1.5$ to 300 K. For evaluation of our point-contact data we need exact values of electrical and thermal conductivity of the sample material, which strongly depend on doping level and crystal perfection; therefore we cannot solely rely on literature parameters, but have to measure the electrical and thermal conductivity as a function of temperature by ourselves. These measurements are also included in this paper.

Measurements of thermal resistance on point contacts provide useful information about heat transport under conditions of boundary scattering. The thermal resistance can in addition be used to calculate the area of the point contact. In this paper we shall mainly concentrate on the latter point, which is of special importance, because the contact area is the most important parameter for interpretation of transport measurements on point contacts.

The contact area is usually calculated from the electrical resistance of the point contact, assuming that the resistance is determined solely by contact geometry.[6] Our measurements of current voltage characteristics and thermopower, however, suggest that electrical tunneling takes place between the two contact legs.[7] This type of transport leads to an additional resistance, which falsifies the calculation of the contact area. As long as the tunnel resistance is small compared with the geometrical resistance, tunneling can be ignored. If the tunnel resistance becomes large, which occurs especially at small contact sizes, then rather severe errors will result. In moderately doped semiconductors heat is almost completely transported by phonons, which are much less sensitive to tunnel barriers than electrons. Calculating the contact area from thermal resistance thus mainly avoids the problems of imperfect surfaces. Comparison of the contact areas, determined from electrical and thermal resistance, provides information about surface perfection and surface purity. Such investigations are only possible at semiconductor point contacts. In metals, where heat transport is mainly carried by electrons, electrical and thermal resistance are similarly affected by tunnel barriers.

A brief introduction into the theory of electrical and thermal transport on microcontacts is given in Sec. II. In Sec. III we describe the experimental arrangement for measurements on bulk samples and point contacts, respectively. The main results are presented and discussed in Sec. IV, and conclusions are drawn in Sec. V.

II. THEORETICAL BACKGROUND

The present standard model for point contacts is a circular orifice in a specular reflecting, isolating plane. The electrical resistance according to this model is well known.[6] There are two limiting cases, depending on the Knudsen number $K=l_e/a$, where l_e is the mean free path of the carriers and a is the contact radius. For $K \ll 1$ (the so-called "Maxwell limit") the macroscopic transport theory is valid, and solving Poisson's equation yields

$$R=\frac{1}{2\sigma a} \quad \text{for } K \ll 1 , \tag{1}$$

where σ is the electrical conductivity. For the Knudsen limit $K \gg 1$, ballistic transport of charge carriers takes place, and the electrical resistance is determined by statistical calculation analogous to kinetic gas theory

$$R = \frac{4K}{3\pi\sigma a} \quad \text{for } K \gg 1 \ . \tag{2}$$

Equation (2) is obtained under the condition that l_e is independent of energy. An interpolation formula between the two limiting cases is given by Wexler under the supposition of elastic and isotropic scattering:[8]

$$R = \frac{\gamma(K)}{2\sigma a} + \frac{4K}{3\pi\sigma a} \ , \tag{3}$$

where $\gamma(K)$ is a slowly varying function with $\gamma(0)=1$ and $\gamma(\infty)=0.694$.

The thermal resistance of the point contact consists of electronic and phononic parts W_e and W_p. In first-order approximation the two parts are independent of each other, and the total thermal resistance becomes

$$W = \frac{W_p W_e}{W_p + W_e} \ . \tag{4}$$

The electronic part W_e can be calculated from the electrical resistance R using the Wiedemann-Franz law

$$W_e = \frac{R}{TL} \ , \tag{5}$$

where T is the temperature and $L = 2.45 \times 10^{-8}\ \mathrm{V^2/K^2}$ is the Lorenz number. Relation (5) is valid even if the contact is covered by an isolating layer and electrical conduction takes place by tunneling.[9] In analogy to Eq. (3) the phononic part of the thermal resistance is[8,10]

$$W_p = \frac{\gamma(K)}{2\kappa a} + \frac{4K}{3\pi\kappa a} \quad \text{with } K = \frac{l_p}{a} \ , \tag{6}$$

where κ denotes the lattice thermal conductivity and l_p is the mean free path of the phonons. In our experiments, W_e always greatly exceeds W_p. Therefore the heat flux through the point contact is carried nearly totally by phonons and the electronic part of the thermal resistance is negligible.

III. EXPERIMENTAL

A. Sample materials

Our experiments are performed on high-purity single-crystalline silicon, which is arsenic doped with a concentration of $1.7 \times 10^{19}\ \mathrm{cm^{-3}}$. This high doping level causes impurity band conduction. Hence the carrier concentration is temperature independent, and the electrical resistivity is governed by impurity scattering. This conclusion is confirmed by our measurements, which shows the electrical conductivity to be almost independent of temperature. The point-contact resistance can thus be measured even at low temperatures, which would not be possible with purer samples because of freezing out of the charge carriers.

B. Bulk measurements

The measurement of electrical and thermal conductivity follows conventional techniques.[11] The specimen is a polished bar with a quadratic cross section of 0.7 $\mathrm{mm^2}$ and a length of about 30 mm. It is cut from the crystal described in Sec. III A with its longitudinal axis parallel to the ⟨111⟩ crystal direction. The specimen is mounted with one end connected to a copper heat sink and a small heater attached to the other. Electrical and thermal connections are made by alloying a thin gold film to the surface of the bar and then soldering onto this film with indium. The absolute temperature is measured by a calibrated Si diode and the temperature gradient along the sample by a difference thermocouple (0.07 at. % Fe in Au versus chromel). The ends of this thermocouple are attached to the bar at a distance of about 12 mm. The thermal anchoring is performed by winding a varnished copper wire several times around the bar and twisting the ends together. The ends are subsequently cleaned from varnish and soldered directly to the thermocouple wires. Finally, the copper wire is glued to the specimen with GE 7031 varnish. This method achieves good thermal contact and fast response in combination with high electrical insulation. Since the electrical leads and the thermocouples are fixed at the same position of the specimen, electrical conductivity, thermal conductivity, and thermopower can be measured simultaneously. The measurements are carried out between 1.5 and 300 K. Heat losses by thermal radiation are measured and taken into consideration. The corrections contribute at most 10% at room temperature.

C. Point-contact measurements

The point contacts are established by pressing two wedge-shaped silicon samples crosswise against each other. The contact area can be changed by variation of the pressure, which is adjusted by a mechanical feed in combination with a piezoelectric drive. The wedges are cut from the crystal described in Sec. III A. The basal plane, which has an area of about $5 \times 3\ \mathrm{mm^2}$, is perpendicular to the ⟨111⟩ crystal direction. The cross section is a rectangular triangle. After polishing, the wedges are etched with CP4 etchant in order to remove surface defects. Directly before mounting the wedges into the cryostat, the oxide layer is removed by dilute HF solution. One of the wedges is connected to a copper heat sink. It is mounted on a small $\mathrm{CuBe_{0.02}}$ spring in order to compensate thermal expansion. The thermal contact to the heat sink is made by flexible copper strand. The second wedge, which is equipped with a small heater, is coupled to the heat sink via a large thermal resistance. This coupling is done by mounting the wedge on two bars of glass-fiber-reinforced polyester, which have a length of 10 mm and a cross section of about 0.1 $\mathrm{mm^2}$.

The whole arrangement is surrounded by a radiation shield on bath temperature. The absolute temperature is measured by calibrated platinum and germanium thermometers. For determination of the temperature difference between the two wedges we use a thermocouple. The thermal resistance $W = \Delta T / \dot{Q}$ is determined by

heating the thermally isolated wedge with constant power $\dot{Q}$ and measuring the resulting temperature difference ΔT, which is adjusted to a few percent of the absolute temperature. To account for residual heat losses, we measure the thermal resistances of the opened and the closed contact W_o and W_c. The point contact resistance W_{pk} thus follows from

$$W_{pk}=\frac{W_o W_c}{W_c-W_o} . \tag{7}$$

Thermal resistance and thermoelectric power as well as electrical resistance are measured simultaneously. The electrical resistance is measured with a fixed voltage of about 20 mV.

IV. RESULTS AND DISCUSSION

A. Bulk measurements

We measure electrical conductivity, heat conductivity, and thermoelectric power of our sample at temperatures from 1.5 to 300 K. The results are in satisfactory agreement with former measurements, carried out on similarly doped material.[12–14] The electrical conductivity of the bulk sample is found to be almost temperature independent: It ranges from 350 $\Omega^{-1}\,\mathrm{cm}^{-1}$ at $T=1.5$ K to 230 $\Omega^{-1}\,\mathrm{cm}^{-1}$ at $T=300$ K. The electronic part of the heat conductivity κ_e is calculated from the electrical conductivity using the Wiedemann-Franz law $\kappa_e=\sigma TL$. The heavy doping of our sample renders L as temperature independent. Inserting the measured values of σ into the Wiedemann-Franz law, we find that κ_e contributes to less then 0.5% to the entire heat conductivity at all temperatures. We therefore neglect κ_e and confine ourselves to the thermal conductivity of the lattice.

Figure 1 shows the measured thermal conductivity. We find considerable differences between our data and the published thermal conductivity of pure silicon,[15] which is represented by a solid line in Fig. 1. Whereas at $T=4$ K the thermal conductivity of the investigated material is about 100 times smaller than that of pure silicon,

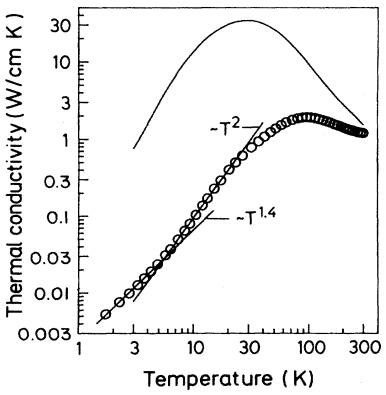

FIG. 1. Thermal conductivity vs temperature. The solid line denotes the thermal conductivity of pure Si measured by Glassbrenner and Slack (Ref. 15).

the values at $T=300$ K are nearly the same. These differences are due to the high doping level of our sample. At high temperatures, the thermal resistivity is dominated by phonon-phonon scattering [*umklapp* (U) processes] independent of doping. At low temperatures, U processes are negligible and other scattering mechanisms become important.[16] There are mainly two mechanisms which occur additionally in doped material: scattering of phonons at impurities and scattering by charge carriers. These two contributions can be distinguished by their temperature dependence:[16] Thermal resistivity due to impurity scattering is proportional to T, scattering by charge carriers varies with T^{-2}. Boundary scattering does not take place, because in the entire temperature range the phonon mean free path is much smaller than the size of the specimen. Scattering by charge carriers therefore is dominant at low temperatures. Impurity scattering becomes important at intermediate temperatures before the onset of U processes. We observe a T^2 law for the thermal conductivity of our sample at temperatures below 20 K. For $T<5$ K we, however, find deviations from the T^2 law which are not yet explained. Similar deviations have also been observed by other authors.[17]

For calculating the radii of our point contacts, we need the mean free paths of electrons and phonons. The phonon mean free path l_p is calculated by means of the well-known kinetic formula of heat conduction

$$\kappa=\tfrac{1}{3}Cvl_p , \tag{8}$$

where C is the lattice specific heat per unit volume and v is the mean sound velocity. Values for C and v are taken from the literature.[18–20] The phonon mean free path calculated by Eq. (8) does not account for details of the phonon spectrum. It represents a mean value about all phonons, weighed by their contributions to thermal conduction. Such an average value is thus well suited for calculation of the thermal resistance of the point contact. For the calculation of the electron mean free path l_e, we use

$$\sigma=\frac{ne^2l_e}{mv} , \tag{9}$$

where n is the carrier density and v is the average electron velocity. Because of the high doping level of our sample we have to replace v by the Fermi velocity v_F. The calculation of v_F is carried out within an impurity band model given by Brody.[21] According to this model we obtain $E_F\simeq 150$ meV and $v_F=\sqrt{2E_F/m^*}=2.3\times10^5$ m/s, where the effective mass m^* is approximated by the free-electron mass. Obviously, Eq. (9) is rather simplified and yields only approximate values of l_e. However, for $K\ll 1$, the inaccuracy of l_e will cause no noticeable mistakes in the calculation of the contact radius, since l_e affects only the Knudsen part of the electrical contact resistance. Figure 2 shows the mean free path of electrons and phonons calculated by Eqs. (8) and (9). Whereas l_e is almost temperature independent, l_p is roughly proportional to $T^{-1.5}$.

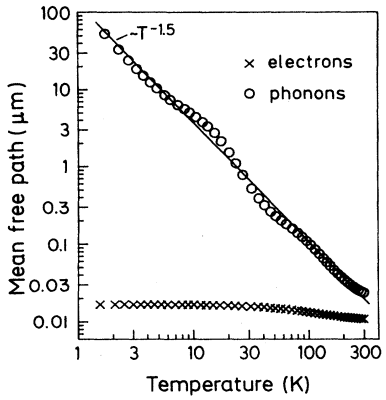

FIG. 2. Electron and phonon mean free path vs temperature. The values are calculated from the measured electrical and thermal conductivity using Eqs. (8) and (9).

B. Point-contact measurements

We investigate the electrical and thermal resistance of the point contact as a function of contact size. The measurements are carried out at various temperatures between 5 and 300 K. From the measured electrical resistance we calculate the contact radius a_e via Eq. (3). The radius a_t is determined from the thermal resistance of the contact using Eq. (4). Since a_t is represented implicitly by Eq. (4), calculations are carried out by numerical zero determination. The mean free paths of the carriers, which enter into calculation, are obtained from Eqs. (8) and (9), respectively. By means of the two contact radii a_e and a_t, we compare electrical and thermal resistance of the point contact directly with each other. This comparison is shown in Fig. 3, where a_t is plotted versus a_e. The presented curves are all measured at the same contact. Though the shape of the curves remains unaffected, the measured data depend considerably on the position of the sample surface, where the point contact is established. Assuming a perfectly clean surface without any defects, we expect a_e and a_t to coincide. This relation $a_t = a_e$, which is represented by a solid line in Fig. 3, actually deviates strongly from the measured data. Whereas at large contact dimensions, a_e and a_t are roughly equal, at small dimensions, a_t is much larger than a_e. For the smallest measured contact, a_t is nearly 30 times a_e. Another important feature, seen in Fig. 3, is the weak temperature dependence of the calculated contact radii. All curves, which belong to temperatures from 1.5 to 300 K, agree within 50%. We thus find a universal empirical law for the relation between a_t and a_e, given by $a_t \sim (a_e)^{0.3}$.

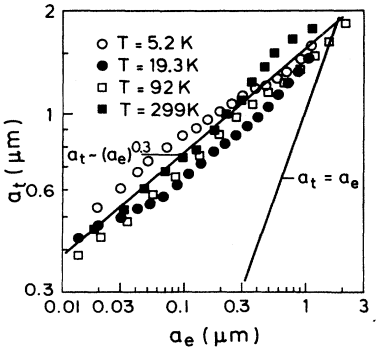

FIG. 3. Contact radius a_t calculated from thermal resistance vs radius a_e calculated from electrical resistance. The solid lines represent the relationship expected for a perfect surface $a_t = a_e$ and the actual dependence $a_t \sim (a_e)^{0.3}$, respectively.

The weak temperature dependence and the magnitude of the measured electrical resistance indicate the existence of a tunnel barrier between the two contact legs, which affects the transport of electrons through the contact. This interpretation is supported by the measured current voltage characteristics, showing a considerable nonlinearity and asymmetry, especially at small contacts.[7] A tunnel resistance is thus generated, which adds to the resistance originating from the geometrical constriction of the point contact. The tunnel resistance falsifies the calculation of the contact radius from electrical resistance, feigning a size a_e smaller than the actual radius. Thus we use the radius a_t, calculated from thermal resistance, as a more reliable measure of the contact size. The accuracy of the calculated a_t values is discussed in the following paragraphs. The tunnel barrier can be regarded, in first-order approximation, as potential barrier of uniform thickness and height. The electrical resistance of the contact thus becomes

$$R = R_{ge} + R_{tu} = \frac{1}{2\sigma a} + \frac{\rho_{tu}}{\pi a^2} . \tag{10}$$

Herein R_{ge} denotes the electrical resistance, originating from the geometrical constriction of the point contact, according to Eq. (1). The second term R_{tu} represents the tunnel resistance. The tunnel resistivity ρ_{tu} is defined as $\lim_{V\to 0} V/j$, where V is the voltage drop across the barrier and j represents the resulting current density.[22] Equation (10) qualitatively agrees with the measured data, since at large contacts R_{ge} exceeds R_{tu}, and a_e represents the actual contact radius. At small contacts, the resistance is dominated by R_{tu}, and a_e becomes smaller than the actual contact size. Qualitatively, however, there are considerable differences between Eq. (10) and the measured relation $R \sim 1/a^{3.3}$, which is easily deduced from Fig. 3 using Eq. (1). To our opinion, these differences are mainly due to the high mechanical pressure at the point contact, which affects the resistivity of the tunnel barrier.

In fact, we know little about the nature of this barrier. The sample surface is covered by an oxide film, which has a thickness of about 12 Å, corresponding to an oxidation time in air of 1 h.[23] With a barrier height of 3.2 eV at the Si/SiO_2 interface[24] this oxide film (total thickness 2×12 Å) provides a tunnel resistivity $\rho_{tu} = 6.6\times 10^5\ \Omega\,\mathrm{cm}^2$.[22] The actual tunnel resistivity of the contact, as calculated from Eq. (10), amounts to $2\times 10^{-7}\ \Omega\,\mathrm{cm}^2 < \rho_{tu} < 10^{-5}$

$\Omega\,\mathrm{cm}^2$. The very large difference between the actual and the calculated value of ρ_{tu} indicates that the oxide film is badly damaged at the contact surface. This statement is supported by experiments in ultrahigh vacuum, on samples cleaned by ion bombardment and analyzed by Auger spectroscopy, which show no significant differences between the electrical properties of clean and oxidized samples.[25] The oxide film can thus not be the only source of the increased contact resistance. Since the effect of adsorbed gases is proved experimentally to be negligible, we believe, that surface states and defects, which trap charge carriers, strongly affect electrical conduction at the contact. Such states are partly generated by the high contact pressure, which ranges up to 2×10^6 N/cm^2, thus exceeding the hardness of silicon, which amounts to 1.13×10^6 N/cm^2. Possibly, the oxide film also contains single conducting regions, which provide a direct connection between the contact legs.

Another effect which affects the contact resistance is the pressure dependence of the electrical conductivity of the sample material. This effect is neglected in our calculations. At constant carrier density—as in our sample—the conductivity of silicon increases with pressure. For the maximal contact pressure of about 2×10^6 N/cm^2 we roughly estimate the conductivity to be six times the value at atmospheric pressure.[26,27] The pressure dependence of the contact resistance is very difficult to calculate, since the pressure is position dependent. A simple calculation, however, indicates that the effect can be estimated using a mean pressure, which is half the maximum pressure at the center of the contact. According to this approximation, the actual values of a_e are somewhat smaller than the values calculated for zero pressure. The differences, which are increasing with pressure, amount to less than a factor of 2.

Similar differences between electrical and thermal resistance, though smaller in magnitude, are observed on metallic point contacts.[3] These differences are interpreted by oxide films and phononic heat transport. In metals, however, electrical and thermal conduction are both affected by tunnel barriers, since heat conduction is mainly carried by electrons. Reliable determination of the contact size is thus very difficult.

So far we maintained that a_t represent the actual contact radius. This is evident, because the thermal resistance is largely dominated by the geometrical constriction of the point contact. The oxide film, being much thinner than the mean free path of phonons, hardly affects thermal conduction. Some effects may nevertheless falsify the calculation of a_t. The high contact pressure may modify the thermal conductivity of the sample in the vicinity of the point contact. Additionally, the calculation of a_t is carried out under several simplifying conditions, as, e.g., circular shaped contact area and uniform mean free path of phonons. These conditions are actually not fulfilled. To check the accuracy of the calculated a_t values, we measure the temperature dependence of the thermal resistance at constant contact load, i.e., at fixed contact size. The measurements are carried out at temperatures from 2 to 50 K. Within this temperature range, the measured thermal resistance varies by more than two decades. Because of the fixed contact size, assuming Eq. (4) to be valid, we expect a_t to be independent of temperature. Figure 4 shows the measured results, obtained for three different values of contact size. We observe a weak decrease of a_t with increasing temperature, which amounts to less than 40% of the value at $T=2$ K. In view of the used simplifications, this agreement is very satisfactory.

As second approach to determine the size of the point contact, we calculate the contact radius from the force, which is applied to the contact legs. As mentioned in Sec. III, one of the wedges is mounted on a small $CuBe_{0.02}$ spring. From the distance of the wedges and the spring resilience, we calculate the contact force. Micrographs of our samples, made by scanning electron microscopy, show the sample edges to be approximately cylindrical shaped, with a radius of about 4 μm. If two cylinders of radius r are pressed crosswise against each other, a spherical contact area arises. The radius of this area is [22]

$$a=1.13\left[\frac{Fr}{E}\right]^{1/3}, \tag{11}$$

where F is the contact force, and E denotes Youngs modulus of elasticity. Equation (11) is valid under the condition of elastic deformation. The mechanical pressure P at the contact is given by

$$P=\frac{3F}{2\pi a^3}(a^2-x^2)^{1/2}, \tag{12}$$

where x is the distance from the center of the contact. The pressure thus reaches its maximum $P=3F/2\pi a^2$ at the center of the contact $x=0$ and vanishes at the contact edge $x=a$. We use contact forces of about 0.001 to 0.2 N, corresponding to pressures of 3.3×10^5 to 1.9×10^6 N/cm^2. Comparing the relation between contact radius a_t and contact force obtained from experiment with Eq. (11), we achieve good correspondence. This result additionally confirms the calculated a_t values. For forces exceeding 0.2 N, we find a considerably stronger depen-

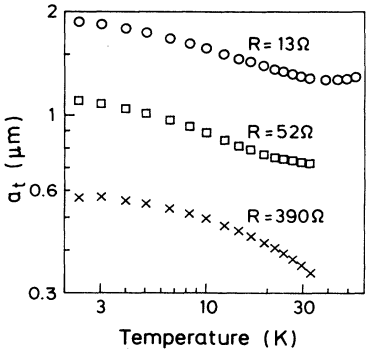

FIG. 4. Contact radius a_t calculated from thermal resistance vs temperature. The curves refer to different values of contact pressure.

dence of contact radius upon load than in Eq. (11). Additionally, the measured data become nonreproducible, presumably due to mechanical destruction of the contact region.

V. CONCLUSIONS

In the present work, we measure for the first time the thermal resistance of silicon microcontacts. Comparison of electrical and thermal transport indicates the existence of a tunnel barrier between the contact legs, which affects electrical conduction. Calculation of the contact radius from electrical resistance thus yields values smaller than the actual geometrical contact size. This discrepancy causes important consequences for any simple-minded conversion of electrical resistance to contact size, as has hitherto been practiced. The problem can be overcome by calculating the contact size from thermal resistance, because in moderately doped silicon heat transport is almost completely carried by phonons. The error in calculating the contact radius from thermal resistance amounts to less than 50%. Measurements of thermal conduction thus represent an improved method to determine the size of semiconductor microcontacts. Additionally, comparison of electrical and thermal resistance provides information about the contact surface. New measurements on weakly doped silicon, which are presently carried out, show even more pronounced differences between electrical and thermal conduction. We also perform measurements to investigate the structure of the tunnel barrier separating the contact legs. These measurements will be discussed in a subsequent publication.

ACKNOWLEDGMENTS

We thank E. Bauser and H. U. Habermeier and their staff for preparation of the samples. R. Trzcinski was always a helpful partner for discussions. This work was partly sponsored by the Stiftung Volkswagenwerk (Hannover, Germany).

[1]I. K. Yanson and O. I. Shklyarevskii, Fiz. Nizk. Temp. **12**, 899 (1986) [Sov. J. Low Temp. Phys. **12**, 509 (1986)].
[2]O. J. Shklyarevskii, A. G. M. Jansen, J. G. H. Hermsen, and P. Wyder, Phys. Rev. Lett. **57**, 1374 (1986).
[3]O. I. Shklyarevskii, A. G. M. Jansen, and P. Wyder, Fiz. Nizk. Temp. **12**, 947 (1986) [Sov. J. Low Temp. Phys. **12**, 536 (1986)].
[4]R. Trzcinski, E. Gmelin, and H. J. Queisser, Phys. Rev. Lett. **56**, 1086 (1986).
[5]R. Trzcinski, E. Gmelin, and H. J. Queisser, Phys. Rev. B **35**, 6373 (1987).
[6]See, e.g., A. G. M. Jansen, A. P. van Gelder, and P. Wyder, J. Phys. C **13**, 6073 (1980).
[7]L. Weber and E. Gmelin (unpublished).
[8]G. Wexler, Proc. Phys. Soc. London **89**, 927 (1966).
[9]M. Kohler, Ann. Phys. (Leipzig) **38**, 542 (1940).
[10]W. A. Little, Can. J. Phys. **37**, 334 (1959).
[11]See, e.g., E. Kaden and H. L. Günter, Phys. Status Solidi B **126**, 733 (1984).
[12]F. J. Morin and J. P. Maita, Phys. Rev. **96**, 28 (1954).
[13]G. A. Slack, J. Appl. Phys. **35**, 3460 (1964).
[14]T. H. Geballe and G. W. Hull, Phys. Rev. **98**, 940 (1955).
[15]C. J. Glassbrenner and G. A. Slack, Phys. Rev. A **134**, 1058 (1964).
[16]J. M. Ziman, *Electrons and Phonons* (Clarendon, Oxford, 1960), pp. 297, 312, and 322.
[17]J. A. Carruthers, T. A. Geballe, H. M. Rosenberg, and J. M. Ziman, Proc. R. Soc. London, Ser. A **238**, 502 (1957).
[18]P. H. Keesom and G. Seidel, Phys. Rev. **113**, 33 (1959).
[19]P. Flubacher, A. J. Leadbetter, and J. A. Morrison, Philos. Mag. **4**, 273 (1959).
[20]H. J. McSkimmin, J. Appl. Phys. **24**, 988 (1953).
[21]T. P. Brody, J. Appl. Phys. **33**, 100 (1962).
[22]R. Holm, *Electric Contacts Handbook* (Springer, Berlin, 1958), pp. 33, 34, and 429–440.
[23]F. Lukes, Surf. Sci. **30**, 91 (1972).
[24]D. R. Young, in *Insulating Films on Semiconductors 1979*, edited by G. G. Roberts and M. J. Morant (Institute of Physics, Bristol, 1980).
[25]R. Trzcinski (private communication).
[26]S. Minomura and H. G. Drickamer, J. Phys. Chem. Solids **23**, 451 (1961).
[27]M. Pollak, Phys. Rev. **111**, 798 (1958).